Flametube Evaluation of a Lean-Lean Combustor Concept Developed for Supersonic Cruise Aircraft

Kathleen M. Tacina
NASA Glenn Research Center
Cleveland, Ohio 44135
Email: kathleen.m.tacina@nasa.gov

Derek P. Podboy
NASA Glenn Research Center
Cleveland, Ohio 44135

Francisco Guzman
NASA Glenn Research Center
Cleveland, Ohio 44135

ABSTRACT

Gaseous emissions were measured in single-cup flametube tests of an advanced low-NO_x combustor concept at simulated supersonic cruise conditions. The combustor concept is a low technology readiness level (TRL), lean front-end design developed under the NASA Fundamental Aeronautics/Supersonics project to minimize NO_x emissions at supersonic cruise. The flametube conditions matched or approached combustor conditions at supersonic cruise, with combustor inlet temperatures up to 920 K, inlet pressures up to 19 bar, and combusted gas temperatures up to 2,120 K. Whether these conditions met or just approached supersonic cruise conditions depended on the type of engine the combustor would be installed in. Two types of engines were considered here: a "derivative" engine based on a current technology and an "advanced" engine with a higher operating pressure ratio and higher temperature limits. For the "derivative" engine, the combustor is expected to be at least close to meeting the NASA NO_x emissions goal of 10 g-NO_x/kg-fuel at supersonic cruise. However, with the higher combustor inlet and flame temperatures of the advanced engine, NO_x emissions are expected to be well above the goal.

1 Introduction

With the recent commercial development of supersonic transports and supersonic business jet by companies such as Boom and Spike [1, 2], there is renewed interest in aircraft engine emissions at supersonic cruise conditions. The emissions of the oxides of nitrogen (NO_x) are of particular concern because NO_x can destroy the protective ozone layer when emitted in the mid to upper stratosphere [3]. NO_x emissions also affect the radiative forcing impacts of supersonic flight [3, 4]. Since ozone and climate impacts depend strongly on the altitude of emissions as well as the assumptions made about the use of supersonic flight (routes, numbers of flights, etc.), atmospheric researchers are simulating the effects of various supersonic flight scenarios [4], where each simulation requires an estimate of the NO_x emissions. This paper reports NO_x emissions measurements needed to develop these estimates for an advanced research combustor.

NO_x emissions depend strongly on combustor technology [5]. This testing uses a radially-staged lean-front-end combustor concept. It is a research Twin Annular Premixing Swirler (TAPS) design developed by GE under NASA's Fundamental Aeronautics/Supersonics program to minimize NO_x emissions at supersonic cruise. This research combustor concept is at a low technology readiness level (TRL); for example, unlike the concepts developed later under NASA's Environmentally Responsible Aviation (ERA) program [6], this TAPS design was not experimentally screened for combustion dynamics or autoignition. Despite the low TRL, this concept can provide reasonable emissions estimates to aid atmospheric researchers in their simulations of the effect of supersonic cruise aircraft on the atmosphere.

NO_x emissions also depend on combustor conditions, which in turn depend on the supersonic cruise altitude, Mach number, and engine cycle. In addition to considering multiple cruise altitudes and Mach numbers, NASA is considering multiple engine cycles [7]. Some cycles are based on in-use engines, while others are advanced clean-sheet cycles. These cycles have significantly different combustor conditions at supersonic cruise. Therefore, we carried out a parametric study

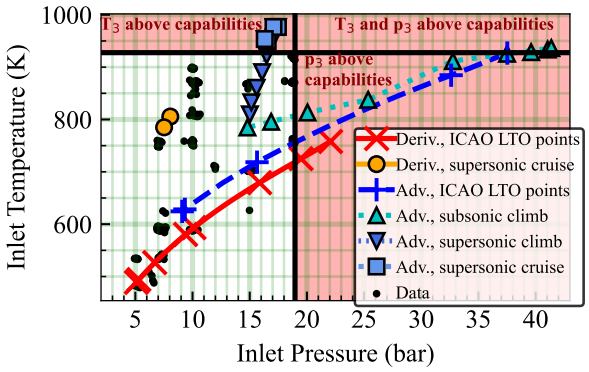

Fig. 1: Combustor inlet temperature and pressure for the two engine cycles used in this paper, the Derivative Cycle ("Deriv.") and the Advanced Cycle ("Adv."). The landing-takeoff (LTO) points are taken on the ground on a test stand (altitude 0, speed 0) and are used for regulating engine emissions. Also shown are the experimental data points. The red shaded area indicates pressure and temperature conditions that cannot be reached in CE-5.

of NO_x as a function of combustor conditions. This will allow NO_x to be estimated for multiple engine cycles and multiple supersonic cruise altitudes and Mach numbers.

Two engine cycles were used to guide the choice of parametrics and to provide example NO_x emissions. Both were created by NASA. The first is a NASA cycle model based on refanning the core of the CFM56 engine to create a mixed-flow turbofan propulsion system capable of Mach=1.4 cruise. This engine, created using publicly available data regarding the CFM56-7B, is called the Derivative Cycle. For the Derivative Cycle, the NO_x emissions from this advanced combustor can be compared to the emissions estimated for a legacy rich-front-end combustor by Berton et al [7]. The second is a NASA cycle model of a more advanced engine cycle with higher operating pressure ration (OPR) and combustor temperature limits; this cycle is called the Advanced Cycle. Both cycles are shown in Fig. 1. To allow for emissions to be evaluated for the two engine cycles given here and yet-to-be developed engine cycles, data are taken at parametric inlet temperatures and pressure instead of the exact inlet temperatures and pressures of the engine cycles.

In addition to their impacts on ozone and climate, NO_x emissions also harm human health. Thus, the NO_x emissions at and near the ground, landing-takeoff (LTO) NO_x, are regulated. Therefore, this paper also reports limited data to compare the LTO NO_x for the Derivative Cycle to the CAEP standard.

2 Experimental Hardware, Facilities, and Data Analysis

2.1 CE-5 Stand 1 Intermediate Pressure Flametube

These tests were done on Stand 1 of the CE-5 intermediate pressure flametube at NASA Glenn Research Center. CE-5 Stand 1 can supply nonvitiated air at pressures up to 19 bar[1]. The maximum preheat temperature is near 920 K; it varies with test cell conditions and decreases somewhat as the air flow rate decreases. CE-5 can provide both Jet-A and alternative aviation fuels; the tests reported here were done with Jet-A.

Although CE-5 Stand 1 can be run as a single-cup sector with realistic liner cooling, it is usually run as a flametube with a cast ceramic liner. The cast ceramic liner typically has a constant or nearly-constant cross-section (e.g., a constant-diameter circle) and is much longer than an aircraft combustor. Although the geometry downstream of the combustor dome is not representative of an actual aircraft combustor, gaseous emissions are estimated reasonably well and so flametube testing is typically used to test a single-cup concept early in combustor development. For the testing described in this paper, a long cast ceramic liner with a nearly-constant cross-section was used to test a single combustor cup.

2.2 Combustor Configuration

This hardware is an experimental version of a TAPS combustor [8] developed by GE under NASA's Fundamental Aeronautics/Supersonics program. It is similar to the configuration reported in Hicks et al [9]. This radially-staged lean-front-end combustor concept has one pilot stage and one main stage. As with all aero-engine combustors, air splits are determined by the geometry; see the cartoon in Fig. 2. In other words, the percentage of air going to the pilot stage, main stage, dome cooling, and liner is fixed by the combustor geometry. Since these flametube tests are done using a cast ceramic liner, all of the air for these tests goes to dome (pilot stage, main stage, or dome cooling, determined by geometry). In an actual combustor, it is assumed that an advanced liner will be used, with 15% to 20% of the total combustor air going

[1] 1 bar = 10^5 Pa = 100 kPa = 0.1 MPa

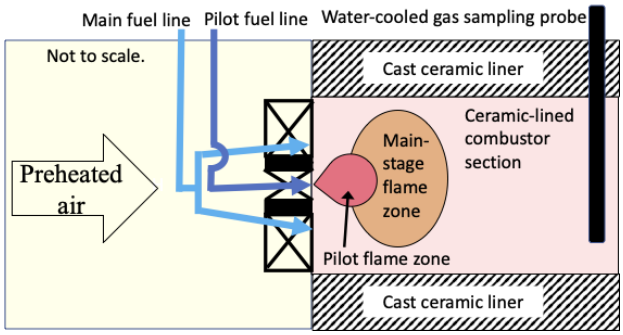

Fig. 2: Cartoon of the combustor hardware as installed in the CE-5 flametube, showing that the fuel splits between the main and pilot stages are controlled by the operator but that the air splits between the main and pilot stages are set by the combustor geometry. Note the fuel lines are drawn to emphasize that the pilot and main fuel can be controlled independently by the test cell operator.

towards liner cooling and the remaining 80-85% of the total combustor air going to the dome. To account for this liner cooling, the flametube equivalence ratio, $\phi_{\text{flametube}}$ is adjusted upwards from the engine equivalence ratio, ϕ_{engine}, using $\phi_{\text{flametube}} = \frac{\phi_{\text{engine}}}{1-0.15}$ to $\frac{\phi_{\text{engine}}}{1-0.20}$.

The fuel flow to the pilot and the main stages can be controlled independently. Fuel staging is accomplished by changing the fuel splits between the pilot and the main stages. The fuel staging is based on the staging presented in Hicks et al [9]. At high power, the fuel staging is typically either 8%, 10%, 15%, or 20% of the fuel going to the pilot and the remainder to the main stage.

2.3 Data Acquisition and Analysis

The NASA Glenn ESCORT real-time data acquisition system was used to collect steady-state data at a rate of 1 Hz. This data acquisition system recorded both facility conditions and gaseous emissions.

Gaseous emissions were collected using a 5-hole water-cooled probe connected to a gas bench. The 5-hole probe was located 34.3 cm downstream of the dome on the combustor centerline. If the gas sampling is representative, the fuel-air ratio calculated using the gaseous emissions should be nearly the same as the fuel-air ratio calculated from the metering of the air and fuel (this ratio is called farr). At the high power conditions that are a focus of this paper, the fuel air ratios are nearly identical: farr has a mean and median of 1.02 and a standard deviation of 0.01. When only the pilot is fueled, farr is further from 1.0, with a mean, median, and standard deviation of 1.17, 1.16, and 0.06, respectively.

The gaseous emissions probe and gas bench followed the SAE ARP1256D [10] standard as closely as possible. One deviation from the standard is the gas sample temperature. The measured combustion products are CO_2, CO, O_2, NO, NO_2, NO_x, and unburned hydrocarbons (UHC). The NO, NO_2, and NO_x measurements were made with two nominally-identical analyzers.

For gaseous emissions, post-processing followed the SAE ARP-1533B [11] standard. As specified by this standard, the combustion efficiency is calculated from the measurements of carbon monoxide and unburned hydrocarbons. Adiabatic combusted gas temperatures and equilibrium CO concentrations are calculated using the Chemical Equilibrium for Applications (CEA) equilibrium code [12, 13].

Each data point consists of at least 60 separate data scans taken at 1-second intervals. Calculations are done at each scan. The data points shown in Fig. 3 through 10 below are an average of all 60+ scans; the error bars represent $\pm$ one standard deviation. The error bars may be difficult to see because they are often smaller than the point markers.

3 Results

This paper focuses on emissions at high power conditions applicable to supersonic cruise. It is organized as follows. First, carbon monoxide emissions and combustion efficiency are summarized. Then, there is a discussion of the dependence of NO_x on four parameters: fuel staging, combustor inlet pressure, combustor inlet temperature, and the pressure drop across the combustor dome as a percentage of combustor inlet pressure. The dependence of NO_x emissions on each of these parameters is shown by comparing sets of curves on plots of NO_x vs. combusted gas temperature in Fig. 4-6. To allow the reader to more easily compare NO_x emissions on the different figures, the scales for the axes are kept constant in these figures. After that, NO_x correlation equations are developed and used to estimate NO_x emissions at supersonic climb and cruise. These NO_x estimates are compared to the data for conditions at which no extrapolation is required. Finally, LTO NO_x emissions for the Derivative cycle are compared to CAEP/8 limits.

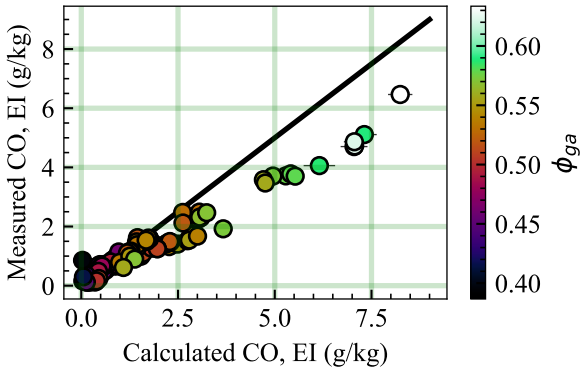

Fig. 3: Measured CO emissions at high power conditions as a function of calculated CO emissions.

3.1 Carbon Monoxide Emissions and Combustion Efficiency

Figure 3 shows measured CO emissions at high power conditions as a function of equilibrium CO as calculated by CEA. CO emissions are generally close to the equilibrium values. Although the measured CO tends to be below the equilibrium value, especially as the emissions index increases, this should not be regarded as significant for two reasons. First, the equilibrium calculations are based on the overall equivalence ratio, not the local equivalence ratio for each fuel stage. Second, the measured CO is near the bottom of the 1,000 ppm range of the analyzer; measured values range from 4 to 331 ppm with a median of 36 ppm. The combustor has acceptable CO emissions that are close to the expected levels.

At high power conditions, the combustion efficiency is high, ranging from 99.83% to 99.99% with a median value of 99.97%.

3.2 Effect of Fuel Staging

Figure 4 shows the effect of fuel staging on NO_x emissions at various combustor inlet temperatures and pressures. Four fuel stagings were primarily considered: 8% of the fuel going to the pilot, 10% of the fuel to the pilot, 15% of the fuel to the pilot, and 20% of the fuel to the pilot. At all conditions, NO_x emissions for the 8% pilot and 10% pilot points were similar. In general, the NO_x emissions for the 15% pilot points were higher than for the 8% and 10% pilot changes, and the NO_x emissions 20% pilot points were higher than for the 15% pilot points. However, as the combusted gas temperature increased, the NO_x emissions for the 15% pilot points and 20% pilot points approached those for the 8% and 10% pilot points.

Two consequences of the effect of fuel staging on NO_x emissions are: (1) to minimize NO_x, 8% or 10% of the fuel should go to the pilot and (2) NO_x correlation equations need to take fuel staging into account.

3.3 Effect of Inlet Pressure

As shown in Fig. 5, inlet pressure has at most a small effect on NO_x emissions. When 8%-10% of the fuel is going to the pilot, increasing combustor inlet pressure may decrease NO_x emissions slightly at lower combusted gas temperatures and increase NO_x emissions slightly at higher combusted gas temperatures. When 20% of the fuel is going to the pilot, combustor inlet pressure has no noticeable effect on NO_x emissions.

The effect of combustor inlet pressure found here is different than for conventional rich-front-end combustors but similar to results from premixed combustors. In rich-front-end combustors, NO_x emissions typically depend on combustor inlet pressure, p_3, as $NO_x \propto p_3^n$, where the pressure exponent n is 0.4-0.8 [5, 14]. However, fundamental studies of premixed combustors [5, 15, 16] give the pressure exponent n as 0 or negative at low flame temperatures (or equivalence ratios), consistent with NO_x formation dominated by the prompt mechanism [5, 15]. At high equivalence ratios, n approaches the value of 0.5, consistent with NO_x formation by the thermal (Zeldovich) mechanism [5, 15]. This lean-front-end TAPS combustor has significant premixing and appears to act more like a premixed flame.

Since the effect of combustor inlet pressure is small for this combustor, the effect of combustor inlet pressure can be neglected for the purposes of estimating NO_x emissions at supersonic cruise.

3.4 Effect of Inlet Temperature

In Fig. 6, sets of curves at differing combustor inlet temperatures show the effect of combustor inlet temperature on NO_x emissions. As expected, NO_x emissions increase as combustor inlet temperature increases.

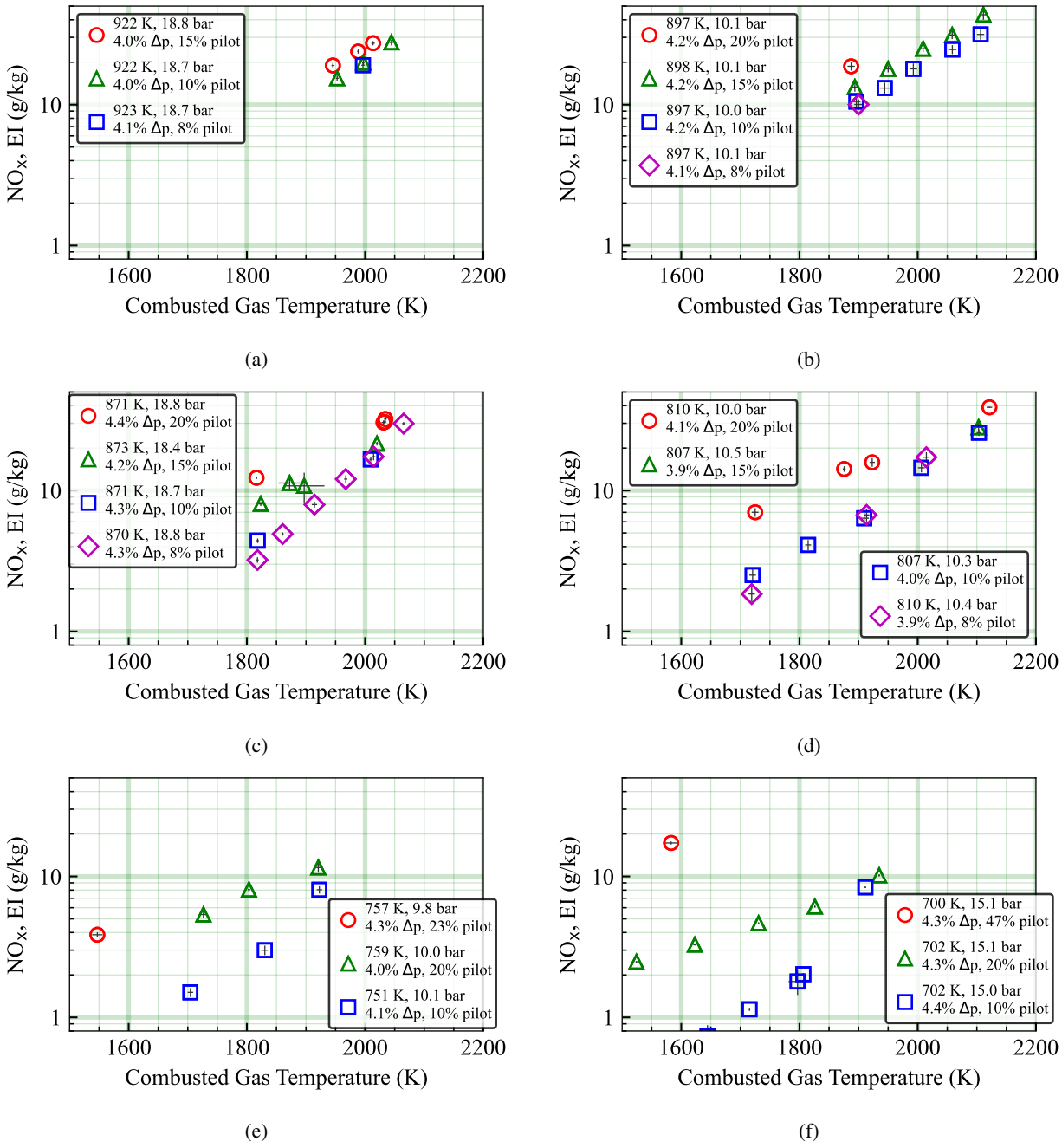

Fig. 4: Effect of fuel staging at various combustor conditions. The values in the legend are combustor inlet temperature, combustor inlet pressure, pressure drop across the combustor dome as a percent of inlet pressure, and percentage of the fuel going to the pilot stage.

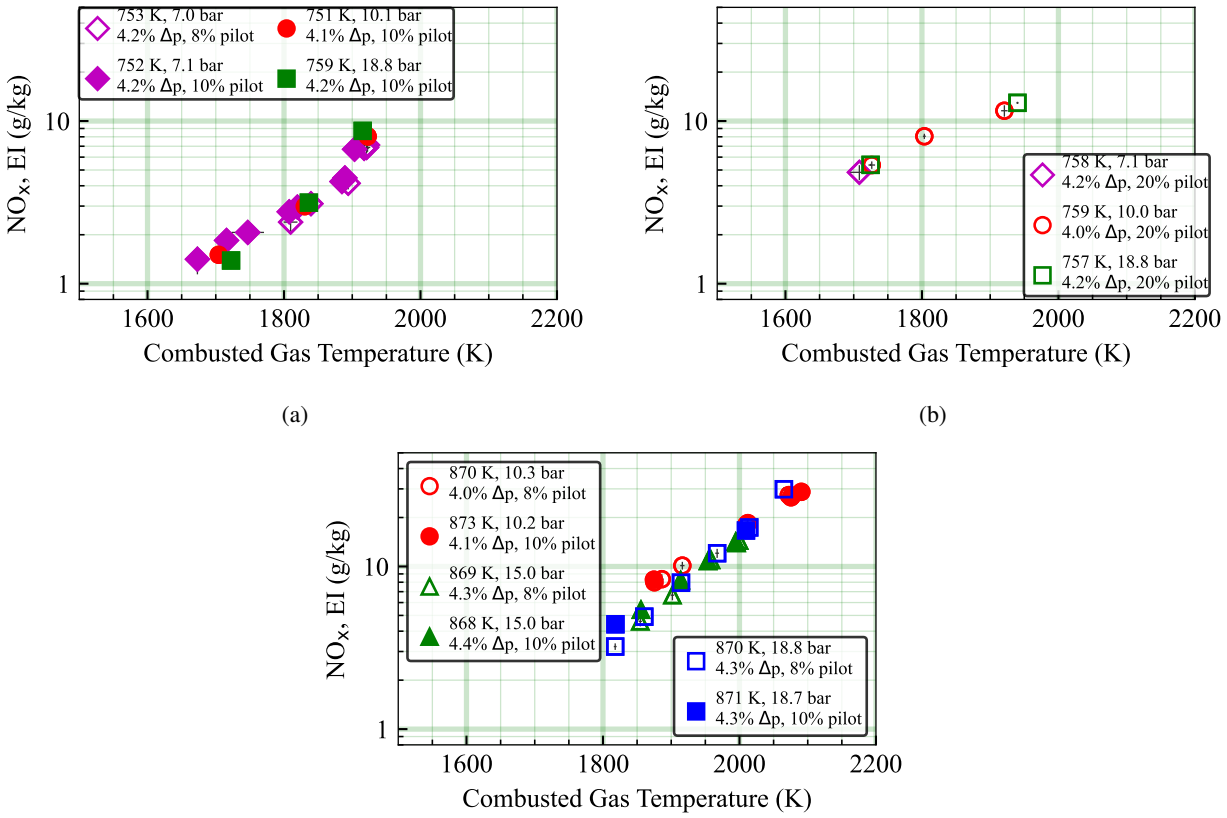

Fig. 5: Effect of combustor inlet pressure on NO_x emissions: (a) inlet temperature near 750 K and 8-10% of the fuel going to the pilot, (b) inlet temperature near 750 K and 20% of the fuel going to the pilot, and (c) inlet temperature near 870 K and 8-10% of the fuel going to the pilot. The values in the legend are combustor inlet temperature, combustor inlet pressure, pressure drop across the combustor dome as a percent of inlet pressure, and percentage of the fuel going to the pilot stage.

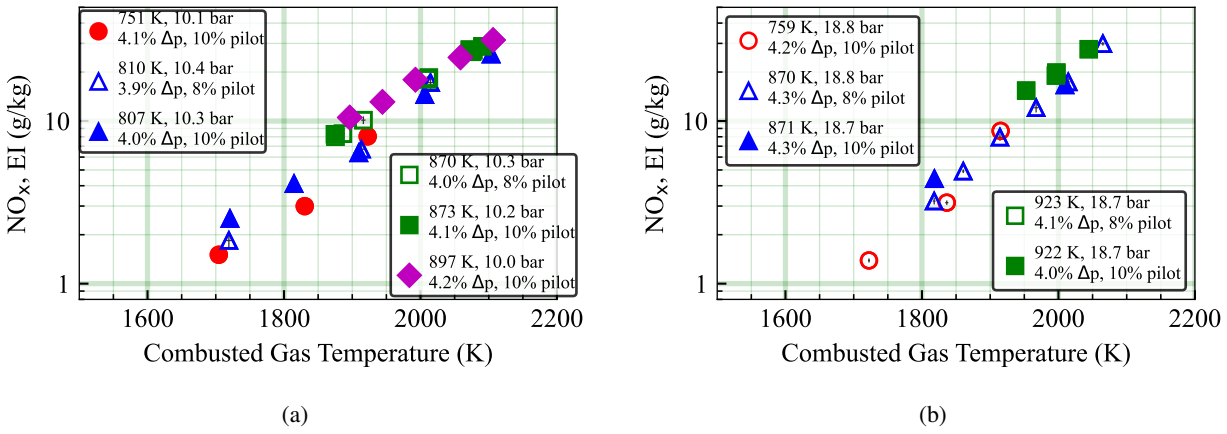

Fig. 6: Effect of combustor inlet temperature on NO_x emissions: (a) inlet pressure of 10 bar and (b) inlet pressure of 19 bar.

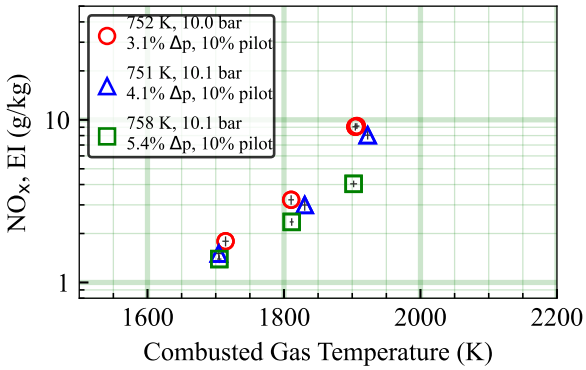

Fig. 7: Effect of dome pressure drop on NO_x emissions.

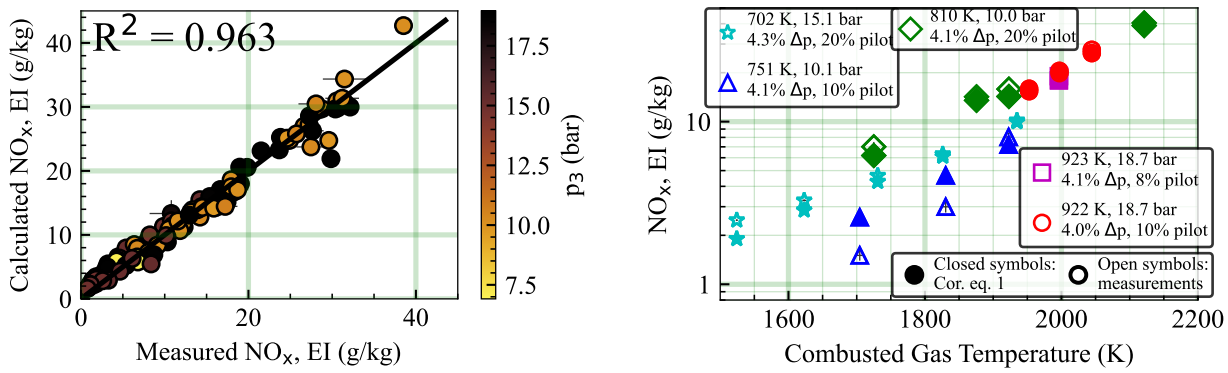

Fig. 8: Evaluation of correlation equation 1, showing (a) calculated NO_x compared to the measured value for all high power points and (b) calculated and measured NO_x as a function of combusted gas temperature for five of the curves shown in Fig. 4.

3.5 Effect of Dome Pressure Drop

Figure 7 shows the effect of the pressure drop across the dome on NO_x emissions. For a given combustor geometry, an increase in the percent pressure drop indicates an increase in the combustor reference velocity. This increased combustor reference velocity decreases the combustor residence time. The decreased residence time should decrease NO_x emissions. However, the increased combustor reference velocity (and thus increased air flow rate) also lead to other changes in the flow, including changes in Weber number and the ratio of air momentum flux to fuel momentum flux. Therefore, the net effect of an increased percent combustor pressure drop is complex. For the TAPS hardware tested here, Fig. 7 shows that higher percent pressure drops decrease NO_x emissions. The decrease in NO_x is highest for the highest pressure drop (5.4%) at 1900 K.

3.6 Correlation Equations and Estimation of NO_x Emissions at Supersonic Cruise

To aid in estimating NO_x emissions at conditions not tested and to provide an equation easily used by engine cycle analysts, correlation equations have been developed. Although these correlation equations cannot be justified from a combustion science perspective, they are useful from an engineering perspective and so are widely used by engine systems analysts and atmospheric researchers to estimate NO_x emissions [14, 17]. With proper entrance pressure, temperature, and fuel/air ratio, the NO_x may be estimated at any point in the flight envelope for the specific combustor design. The form chosen for these correlation equations is based on correlation equations developed by the authors for other lean-front-end combustion concepts [18] and is similar to correlation equations developed by other groups [14].

The form of the correlation equations below was also based on the parametric results described above. Those results showed that the combustor inlet pressure had at most a small effect on NO_x emissions, so it was left out of the correlation equations. Combustor inlet temperature and the percent pressure drop across the dome did have a significant effect on NO_x emissions, so the correlation equations included the effects of these variables. Fuel staging also had a significant effect on

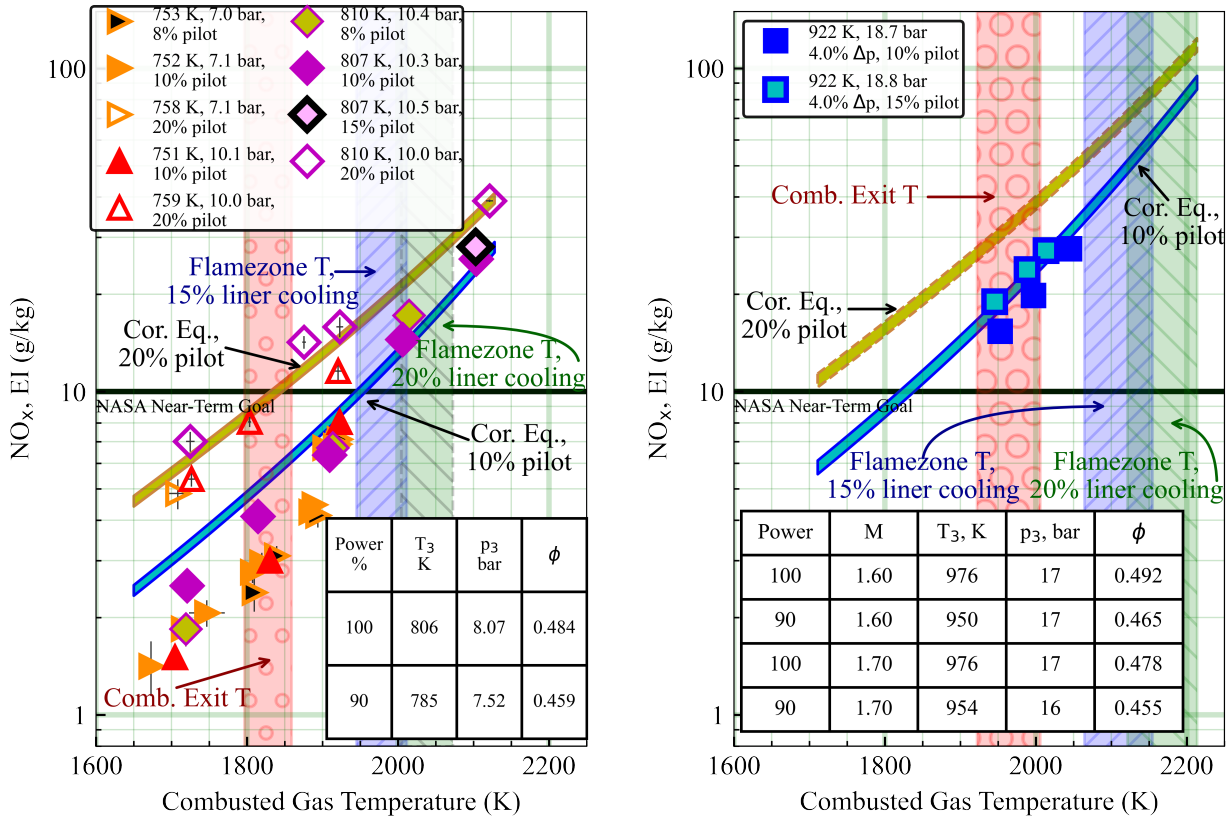

Fig. 9: NO_x at supersonic cruise for (a) the Derivative Cycle and (b) the Advanced Cycle.

Table 1: SUPERSONIC CRUISE CONDITIONS Given are the supersonic cycle, Mach number, altitude, engine power setting, the combustor conditions, the combusted gas temperature in the flame zone when adjusted for 15% and 20% liner cooling, the NO_x emissions estimated using the correlation equation, NO_x emissions estimated directly from curves shown in Fig. 6.

Cycle	Alt	Mach	Power Setting	p_3	T_3	ϕ_{engine}	$T_{comb\ gas}$ 15% l.c.	$T_{comb\ gas}$ 20% l.c	Est. NO_x	Meas. NO_x
	km		%	bar	K		K	K	g/kg	g/kg
Derivative	15.2	1.4	100	8.1	805	0.484	2,010	2,071	14-20	14-20
Derivative	15.2	1.4	90	7.5	785	0.459	1,945	2,004	9.4-13	7-14
Advanced	15.2	1.6	100	17.4	976	0.492	2,155	2,214	64-94	
Advanced	15.2	1.6	90	16.5	950	0.465	2,082	2,140	37-53	
Advanced	15.5	1.7	100	17.1	976	0.478	2,129	2,187	54-78	
Advanced	15.5	1.7	90	16.3	954	0.455	2,064	2,121	34-47	

NO_x emissions, so the fractions of fuel going to the pilot and main stages was included. The form of the equation is:

$$\mathrm{eiNO_x} = 0.001 e^{\frac{T_3}{a}} \left(b \mathrm{X_{pil}}\, e^{\frac{T_{\mathrm{comb\ gas}}}{c}} + d \mathrm{X_{main}}\, e^{\frac{T_{\mathrm{comb\ gas}}}{f}} \right) \Delta p^g, \quad (1)$$

where $\mathrm{eiNO_x}$ is the NO_x emissions index in g/kg, T_3 is the combustor inlet temperature in Kelvin, $\mathrm{X_{pilot}}$ is the *fraction* of fuel going to the pilot stage, $\mathrm{X_{main}}$ is the fraction of fuel going to the main stage, Δp is the combustor pressure drop as a *percentage* of the inlet pressure, and $T_{\mathrm{comb\ gas}}$ is the overall combusted gas temperature in Kelvin. The correlations were determined using a least squares curve fit to the data and are as follows: a=274±1.4 K, b=6.47±0.27, c=264±1.6 K, d=3.05×10^{-5} ±4.1 × 10^{-6}, f=117±0.84 K, g= -0.736±0.014. NOx emissions from this correlation equation are compared to the measured emissions in Fig. 8. The correlation equation captures the NO_x emissions reasonably well, with a R^2 value of 0.963. Thus, the correlation equation equations can be expected to provide a reasonable estimate of NO_x emissions for atmospheric studies. For these studies, a rough estimate of the NO_x is frequently used: the question is not whether, for example, NO_x is 4.8 or 5.2 g/kg, but whether NO_x is more like 5, 10, 20, or 40 g/kg.

These equations are used to estimate NO_x emissions at supersonic climb and cruise. Results are given in Table 1. For conditions where no extrapolation on inlet temperature or combusted gas temperature is required, NO_x emissions are also estimated from the curves shown in Fig. 6. As this comparison shows, the estimates from the correlation equations agree reasonably well with the data. For the Derived cycle, the NO_x emissions meet or are close to NASA program goals of 10 g-NO_x/kg-fuel. However, for the Advanced cycle, the supersonic cruise emissions are well above this goal.

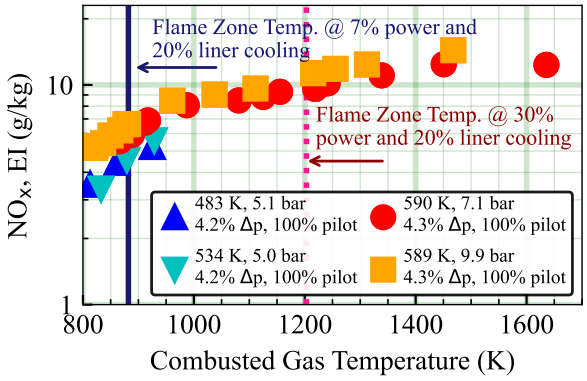

Fig. 10: NO_x emissions at the LTO 7% and 30% power settings for the Derivative cycle.

3.7 Landing-Takeoff Cycle Emissions Estimates

Table 2: ICAO LTO cycle, combustor conditions for the derived cycle, and corresponding gaseous emissions and combustion efficiency.

ICAO power setting	Time	Fuel flow	T_3	p_3	ϕ_{eng}	$T_{\mathrm{comb\ gas}}$ 20% l.c.	NO_x, EI	CO, EI	UHC, EI	η_c
	(min)	(kg/min)		(K)	(bar)	(K)	(g/kg)	(g/kg)	(g/kg)	(%)
7%	26.0	5.9	494	5.3	0.117	882	4.7	27	2	99.2
30%	4.00	15.3	582	9.4	0.201	1,203	10.8	7	0.2	99.8
85%	2.20	46.6	725	19.5	0.355	1,720	1.2	0.2	0	99.99
100%	0.700	56.5	758	22.1	0.394	1,838	3.2	0.5	0	99.99

Although NO_x emissions near the ground represent only a small fraction of the total NO_x emissions, low altitude NO_x emissions exert an adverse effect on human health by contributing to ground level smog and ozone. Therefore, ICAO has established limits on the emissions of pollutants below 918 m (3,000 ft). The ICAO limits are evaluated over a standard LTO cycle and expressed in terms of the NO_x severity parameter (D_p/F_{00}), the rated thrust of the engine (F_{00}), and the operating pressure ratio at takeoff (π_{00}). D_p/F_{00} is calculated using

$$D_p/F_{00} = \frac{1}{F_{00}} \sum_i t_i w_{f,i} \mathrm{EINOx}_i, \tag{2}$$

where i refers to the ICAO power setting, t_i is the time at that power setting as defined in the CAEP/6 standard and given in Table 2, $w_{f,i}$ is the fuel flow, and EINOx_i the NO_x emissions index. ICAO has defined standards for LTO points for both subsonic cruise and supersonic cruise aircraft, but the standard for supersonic cruise aircraft has not been updated since the Concorde was certified. Due to this lack of updates and to the expectation that the new standard for supersonic cruise aircraft will be based on a subsonic standard, we will compare the estimated LTO NO_x emissions to the current subsonic standard. The Derived cycle will be used for this comparison.

The ICAO power settings, the time at each setting, and the Derived cycle conditions and estimated emissions are given in Table 2. For the derived cycle, F_{00} is 73.9 kN (16,618 lbf), leading to a D_p/F_{00} of 21.7 g/kN. The allowable NO_x depends on F_{00} and π_{00}, which is 21.7 for the Derived cycle. For the current CAEP/8 standard, the maximum allowable NO_x is

$$D_p/F_{00} = 40.052 + 1.5681\pi_{00} - 0.3615F_{00} - 0.0018\pi_{00} \times F_{00}, \tag{3}$$

which 45 g/kN. Thus, the estimated D_p/F_{00} for this engine test is 50% below the CAEP/8 standard. Although NO_x is expected to change somewhat when going from a flametube test of a single cup design with unrealistic liner cooling (like the cast ceramic flametube here, with no liner cooling) to a multi-cup annular design, the NO_x emissions are still expected to be below the CAEP/8 standard.[2]

3.8 Discussion

As these results show, the NO_x emission index at supersonic cruise depends strongly on the supersonic cruise conditions and the engine cycle. For the Advanced Cycle cruising at Mach 1.6- 1.7 and 15.2-15.5 km, the NO_x emission index is 3-10 times higher than the NASA goal of 10 g-NO_x/kg-fuel. However, for the Derivative Cycle cruising at Mach 1.4 and 15.2 km, the NO_x emission index meets or is close to the goal. Although an decrease in combustor inlet temperature contributes to the decrease in NO_x emissions when going from the Advanced Cycle to the Derivative Cycle, the primary driver is the decrease in flame zone temperature.

Since thermal NO_x is an exponential function of local, instantaneous flame temperature at fuel-lean conditions, this large decrease in NO_x emissions when comparing supersonic cruise emissions from the Advanced to the Derivative Cycle would be expected in other lean-front-end combustor concepts. This is indeed the case for two variations of another lean-frontend concept, lean direct injection (LDI) — despite significant differences between TAPS and LDI combustors. Although both TAPS and LDI are lean-front-end combustor concepts, LDI combustor geometry is considerably different than the TAPS geometry. For example, in LDI, multiple fuel-air mixers replace a single TAPS fuel-air mixer. Another significant difference is that the NO_x emissions from LDI combustors depend on pressure; this pressure dependence indicates that in LDI the combustion is not premixed. Despite these differences, LDI also has a large decrease in NO_x emissions when going from the Advanced Cycle to the Derivative Cycle. Two LDI designs, the second-generation "5-recess" design in Reference [19] and the third-generation design in References [18] and [20], were tested in the same flametube at conditions approaching the Advanced Cycle supersonic cruise at 90% power and Mach 1.7, with 15% liner cooling. For both of these LDI designs, NO_x emissions are expected to be near 40 g/kg at this Advanced Cycle condition. However, for the Derivative Cycle supersonic cruise at 90% power and Mach 1.4, with 15% liner cooling, the NO_x emissions are expected to decrease to below 10.

As Table 1 and Fig. 9 show, changes to the fraction of combustor air required for combustor liner cooling significantly affect NO_x emissions. Increasing the amount of combustor air required for liner cooling does not change the overall fuel-air ratio. However, because the air used to cool the combustor liner is not available to mix with the fuel, the fuel-air ratio in the flame zone will increase. The increased flame zone fuel-air ratio leads to increased NO_x emissions. Since the NO_x correlation equation developed in this paper (eq. 1) uses the combusted gas temperature in the flame zone, it can be used to estimate the effect of liner cooling on NO_x emissions.

[2] Due to the focus on supersonic cruise emissions and the limited testing time, the number of low power points were limited and the Derivative cycle was given priority. For the Advanced cycle, it is estimated that this design will meet the CAEP/4 standard, be close to the CAEP/6 standard, and be above the CAEP/8 standard. However, the results for the Advanced cycle should be viewed with skepticism because of the uncertainty of the NO_x emissions for the 30% and especially the 7% power points.

However, the NO_x emissions index is not the only determinant of the effects of supersonic cruise NO_x emissions on the protective ozone layer. A more efficient engine and airframe could reduce the total amount of NO_x emitted at supersonic cruise even if the emissions index is higher. In addition, as discussed in length in Speth et al [21], the effect of NO_x emissions on the ozone layer depends not only on the actual emissions but also on other factors such as altitude.

The climate effects of supersonic flight are also complex. For example, NO_x emissions change the effect radiative forcing of aviation by interacting with methane and stratospheric water vapor as well as ozone [22]. As another example, contrails at the higher altitudes of supersonic cruise are expected to last longer than current contrails from subsonic aircraft — but they are also expected to form less often, so replacing subsonic flights with supersonic flights may actually decrease the warming from contrails [21]. Since contrails are the greatest contributor to short-term warming from aviation, surpassing even carbon dioxide emissions [22], better understanding the formation of contrails for both supersonic- and subsonic-cruise aircraft are needed to understand the climate impact of a supersonic cruise fleet.

Therefore, understanding the effect of a supersonic cruise passenger fleet on the ozone layer and the climate requires integrated modeling, combining emissions estimates such as the one provided in this paper with engine cycle analysis, fleet modeling, and climate simulations. The correlation equation developed in this paper can be used to estimate NO_x emissions not only for the engine cycle reported in this paper but for other engine cycles. Only the combustor conditions and an estimate of the fraction of combustor air used for combustor liner cooling are needed. Similarly, if engine cycle calculations are done using atmospheric conditions that deviate from the standard atmosphere, the correlation equation can estimate the NO_x emissions at those conditions.

4 Summary

A lean-front-end experimental combustor concept was tested in a ceramic-lined flametube. NO_x emissions were measured at combustor conditions approximating supersonic cruise. Using these measurements, a correlation equation was developed to predict NO_x emissions as a function of combustor conditions. The measurements and correlation equation were then used to estimate cruise NO_x emissions for two engines, an engine based on a currently in-service engine, with the Derivative Engine Cycle, and an advanced engine, with the Advanced Engine Cycle. NO_x emissions at multiple supersonic climb and cruise conditions were estimated using both the measurements and the correlation equation. Cycle operating conditions play a dominating role in NO_x emissions, with NO_x emission indices at supersonic cruise ranging from 7 to 14 g/kg for the Derivative Cycle and from 34-94 g/kg for the Advanced Cycle. These results can be combined with modeling of the engine, aircraft, and probable supersonic fleet size and routes to determine the effect of a supersonic passenger fleet on the protective ozone layer and the environment.

References

[1] Adams, E., 3 April 2019. "Even if you missed out on the concorde, you may soon get a chance to fly in a supersonic airliner". *Popular Science*.

[2] , 2021. Will supersonic passenger planes fly again?

[3] Seinfeld, J. H., and Pandis, S. N., 2006. *Atmospheric Chemistry and Physics: From Air Pollution to Climate Change*, 2 ed. John Wiley & Sons, Inc., Hoboken, New Jersey.

[4] Grewe, V., Plohr, M., Cerina, G., Di Muzio, M., Deremaux, Y., Galerneau, M., de Saint Martin, P., Chaika, T., Hasselrot, A., Tengzelius, U., and Korovkin, V., 2010. "Estimates of the climate impact of future small-scale supersonic transport aircraft — results from the HISAC EU-project". *The Aeronautical Journal,* **114**(1153).

[5] Lefebvre, A. H., 1998. *Gas Turbine Combustion*, 2nd ed. Taylor and Francis, Philadelphia.

[6] Herbon, J., Aicholtz, J., Hsieh, S.-Y., Viars, P., Birmaher, S., Brown, D., Patel, N., Carper, D., Cooper, C., Fitzgerald, R., Pandalai, R., and Hong, Z., 2017. N+2 advanced low NOx combustor technology final report. NASA/CR-2017-219410.

[7] Berton, J. J., Huff, D. L., and Seidel, J. A., 2020. Supersonic technology concept aeroplanes for environmental studies. AIAA-2020-0263.

[8] Foust, M. J., Thomsen, D., Stickles, R., and Dodds, W., 2012. Development of the GE Aviation low emissions TAPS combustor for next generation aircraft engines. AIAA 2012-0936.

[9] Hicks, Y. R., Tedder, S. A., and Anderson, R. C., 2016. Alternative bio-derived JP-8 class fuel and JP-8 fuel: Flame tube combustor test results compared using a GE TAPS injector configuration. AIAA-2016-4890.

[10] SAE E-31 Technical Committee, 2011. Procedure for the continuous sampling and measurement of gaseous emissions from aircraft turbine engines. SAE ARP 1256D.

[11] SAE E-31 Technical Committee, 2013. Procedure for the analysis and evaluation of gaseous emissions from aircraft engines. SAE ARP 1533B.

[12] McBride, B., and Gordon, S., 1992. Computer program for calculating and fitting thermodynamic functions. NASA RP-1271.

[13] McBride, B., Zehe, M., and Gordon, S., 1993. NASA Glenn coefficients for calculating thermodynamic properties of individual species. NASA TP-3287.

[14] Chandrasekaran, N., and Guha, A., 2012. "Study of prediction methods for NOx emissions from turbofan engines". *Journal of Propulsion and Power,* **28**, pp. 170–180.

[15] Nicol, D., Malte, P. C., Lai, J., Marinov, N. N., Pratt, D. T., and Corr, R. A., 1992. NOx sensitivities for gas turbine engines operated on lean-premixed combustion and conventional diffusions engines. 92-GT-115.

[16] Rutar, T., and Malte, P., 2002. "NO_x formation in high-pressure jet-stirred reactors with significance to lean-premixed combustion turbines". *Transactions of the ASME,* **776**.

[17] DuBois, D., and Paynter, G. C., 2006. ""Fuel Flow Method2" for Estimating Aircraft Emissions". *SAE Transactions: Journal of Aerospace,* **115**, pp. 1–14.

[18] Tacina, K., Podboy, D., Lee, F., and Dam, B., 2017. Gaseous emissions results from a three-cup flametube test of a third-generation swirl-venturi lean direct injection combustion concept. ISABE-2017-22606.

[19] Tacina, K. M., Lee, P., Mongia, H., Chang, C. T., He, Z., and Dam, B., 2014. A second generation swirl-venturi lean direct injection combustion concept. AIAA 2014-3434.

[20] Ajmani, K., Lee, P., Chang, C. T., and Kudlac, M. T., 2019. CFD evaluation of lean-direct injection combustors for commercial supersonics technology. AIAA 2019-4199.

[21] Speth, R. L., Eastham, S. D., Fritz, T. M., Inés Sanz-Morère, A. A., Prashanth, P., Allroggen, F., and Barrett, S. R., 2021. Global environmental impact of supersonic cruise aircraft in the stratosphere. NASA/CR-20205009400.

[22] Lee, D., Fahey, D., Skowron, A., Allen, M., Burkhardt, U., Chen, Q., Doherty, S., Freeman, S., Forster, P., Fuglestvedt, J., Gettelman, A., Le´on, R. D., Lim, L., Lund, M. T., Millar, R., Owen, B., Penner, J., Pitari, G., Prather, M., Sausen, R., and Wilcox, L. J., 2021. "The contribution of global aviation to anthropogenic climate forcing for 2000 to 2018". *Atmospheric Environment,* **244**.

[23] Walt, S. v. d., Colbert, S. C., and Varoquaux, G., 2011. "The numpy array: A structure for efficient numerical computation". *Computing in Science and Engineering,* **13**(2), pp. 22–30.

[24] Jones, E., Oliphant, T., Peterson, P., et al., 2001–. SciPy: Open source scientific tools for Python. [Online; accessed 26 October 2018].

[25] Hunter, J. D., 2007. "Matplotlib: A 2d graphics environment". *Computing In Science & Engineering,* **9**(3), pp. 90–95.

[26] McKinney, W., 2010. "Data structures for statistical computing in python". In Proceedings of the 9th Python in Science Conference, S. van der Walt and J. Millman, eds., pp. 51 – 56.

[27] Pérez, F., and Granger, B. E., 2007. "IPython: a system for interactive scientific computing". *Computing in Science and Engineering,* **9**(3), May, pp. 21–29.

Acknowledgements

This work was supported by the National Aeronautics and Space Administration's Commercial Supersonic Technology project. Thanks to Jeffrey Berton and Jonathan Seidel for providing cycle information. Thanks to the engineering and technician staff at the NASA CE-5 flametube rig. Thanks also to the open-source software community for providing the software used for data analysis: numpy [23], scipy [24], matplotlib [25], pandas [26], ipython [27], and jupyter notebook.

List of Tables

List of Figures